

A Flexible and Biodegradable Piezoelectric-Based Wearable Sensor for Non-Invasive Monitoring of Dynamic Human Motions and Physiological Signals

Mohsin Ali, Seyed Morteza Hoseyni, Ritu Das, Muhammad Awais, Ipek Basdogan, and Levent Beker*

Recent progress in flexible sensors and piezoelectric materials has enabled the development of continuous monitoring systems for human physiological signals as wearable and implantable medical devices. However, their non-degradable characteristics also lead to the generation of a significant amount of non-decomposable electronic waste (e-waste) and necessitate a secondary surgery for implant removal. Herein, a flexible and biodegradable piezoelectric material for wearable and implantable devices that addresses the problem of secondary surgery and e-waste while providing a high-performance platform for continuous and seamless monitoring of human physiological signals and tactile stimuli is provided. The novel composition of bioresorbable poly(L-lactide) and glycine leads to flexible piezoelectric devices for non-invasive measurement of artery pulse signals in near-surface arteries and slight movement of the muscle, including the trachea, esophagus, and movements of joints. The complete degradability of piezoelectric film in phosphate-buffered saline at 37 °C is also shown. The developed pressure sensor exhibits high sensitivity of 13.2 mV kPa⁻¹ with a response time of 10 ms and shows good mechanical stability. This piezoelectric material has comparable performance to commonly used non-degradable piezoelectric materials for measuring physiological signals. It can also be used in temporary implantable medical devices for monitoring due to its degradable nature.

1. Introduction

Continuous monitoring of physiological signals via biomedical devices in daily life has received significant attention.^[1–3] High-accuracy monitoring of human physiological signals^[4,5] in addition to the body motions,^[6,7] is feasible through the seamless integration of the device with the skin or tissue of the human body. This way, several biomedical devices have been demonstrated with various transduction principles, including electrostatic, piezoelectric, capacitive, and piezoresistive effects.^[8–10] To this extent, devices based on the piezoelectric effect hold a critical promise in advanced human-machine interface devices compared to other devices owing to the various advantages, including self-powered ability, flexible form factor, high sensitivity, and facile fabrication. Various flexible pressure sensors have been studied to measure the physiological signals generated by human activities. However, supplying voltage to operate these devices is a crucial barrier for developing

M. Ali, M. Awais
Department of Biomedical Sciences and Engineering
Koç University
Rumelifeneri Yolu, Sariyer, Istanbul 34450, Turkey

S. M. Hoseyni, R. Das, I. Basdogan, L. Beker
Department of Mechanical Engineering
Koç University
Rumelifeneri Yolu, Sariyer, Istanbul 34450, Turkey
E-mail: lbeker@ku.edu.tr

L. Beker
Koç University Research Center for Translational Research (KUTTAM)
Rumelifeneri Yolu, Sariyer, Istanbul 34450, Turkey

 The ORCID identification number(s) for the author(s) of this article can be found under <https://doi.org/10.1002/admt.202300347>

© 2023 The Authors. Advanced Materials Technologies published by Wiley-VCH GmbH. This is an open access article under the terms of the Creative Commons Attribution-NonCommercial-NoDerivs License, which permits use and distribution in any medium, provided the original work is properly cited, the use is non-commercial and no modifications or adaptations are made.

The copyright line for this article was changed on 22 August 2023 after original online publication.

DOI: 10.1002/admt.202300347

energy-efficient wearable sensors.^[11,12] Additionally, frequent replacement of the power source limits the application of wearable and implantable electronics for both in vivo and in vitro environments.^[13] As an alternative, a self-powered pressure sensor has the potential to resolve the issue related to power consumption for future wearable healthcare sensors. In this sense, pressure sensors based on piezoelectric^[14,15] and triboelectric effects^[16–18] can directly produce electricity with external force, enabling the realization of a self-operating sensor. Triboelectric-based devices operate based on the triboelectric effect and electrostatic induction. Triboelectric-based devices operate based on the triboelectric effect and electrostatic induction. Although electrostatic charges produced by the friction (triboelectric effect) are ideal for force sensing and energy harvesting applications,^[19] but has some downsides including the variation in the force response because of the delay of charge dissipation in the sensor,^[20] are commonly vulnerable to noise from the motion of the sensor,^[21] and a restriction of miniaturization owing to the obligation of keeping a physical gap between triboelectric layers. Moreover, the triboelectric sensor is vulnerable to humidity, limited bio-signal detection, complex fabrication, and short dynamic range because of the low sensitivity under increased applied load and abrasion resistance.^[22–24]

Piezoelectric devices made of inorganic piezo materials such as PZT and BaTiO₃ have been demonstrated as efficient health monitoring devices in various applications.^[25–28] However, the problem with these devices made of piezoceramic materials is the toxicity of some of the components, especially PZT ceramics. Compared to piezo ceramics, piezoelectric polymers exhibit good compatibility with the environment and high flexibility.^[29] Piezoelectric polymers have been reported in the manufacturing of transducers and force/pressure sensors.^[30,31] Yuan et al. fabricated a composite piezoelectric material based on poly(vinylidene fluoride) (PVDF) and ZnO to detect human elbow flexure.^[32] PVDF is the most commonly used flexible and piezoelectric polymer demonstrating high piezoelectricity compared to other piezoelectric polymers.^[33] However, it is not as suitable as the eco-friendly material because it contains non-degradable components and waste produced by these materials is considered a threat to our environment.^[29] Emerging applications in wearable and implantable health monitoring systems require self-powered biodegradable devices to monitor the physiological state of the human body.^[34,35] Simple and low-temperature processing of naturally-driven biodegradable and biocompatible piezoelectric materials such as peptide nanotubes, cellulose, collagen, and amino acids have received significant interest.^[36–38] However, the low stability of natural biodegradable piezo materials^[39] and their irregular arrangements leading to low output voltage in the film have limited their use in real-time applications. Although biodegradable glycine (Gly) based amino acids have recently been reported with a high piezoelectric coefficient,^[40] fabricating functional thin films with controllable piezoelectricity from these powder-based materials is challenging.

In the case of a synthetically biodegradable piezoelectric polymer, poly(L-lactide acid) (PLLA) has received attention because of its excellent biocompatibility and biodegradability in biomedical devices such as FDA-approved implants and biodegradable force sensors.^[41–46] Although PLLA exhibits modest piezoelectricity (5–15 pC/N) and has a low dielectric constant, it provides energy

conversion efficiency similar to commercial piezoelectric polymer PVDF.^[42,47] PLLA-based piezoelectric devices, such as filtration devices, smart fabric, pressure sensors, and actuators, have been developed for biomedical applications.^[48–50] Curry et al. thermally stretched bulk PLLA films to generate piezoelectricity. However, problems were observed, like film rigidity and low reproducibility,^[51,52] which makes stretched PLLA film insensitive for sensitive pressure sensors, transducers, and actuators. To overcome the challenges mentioned above, a flexible, biodegradable piezoelectric film with a stable piezoelectric response and stretch-free fabrication is needed that can be facilely fabricated and has a high potential to be implemented in various sensing applications.

Herein, we present a flexible and biodegradable piezoelectric film based on the novel composition of PLLA/Gly with a stretch-free fabrication process and controllable piezoelectricity, for self-powered monitoring of physiological signals. We demonstrate the ability of the sensor to detect human physiological signals, such as carotid and radial artery signals, as well as tactile stimuli, such as wrist and elbow movement, coughing, and swallowing actions. We also show the biodegradability of piezoelectric PLLA/Gly film in phosphate-buffered saline (PBS) at 37 °C. Despite of the several achievements in biodegradable electronics,^[34,53,54] this study introduces an easy-to-fabricate, flexible, highly efficient, and biodegradable piezoelectric material, which is only made of bioresorbable materials being used for medical applications. The newly fabricated bioresorbable piezoelectric material could be a potential candidate for developing self-powered wearable and implantable sensing devices.

2. Result and Discussion

Figure 1 illustrates the fabrication process of the flexible piezoelectric film and wearable pressure sensor, the biodegradability of piezoelectric PLLA/Gly film, and real-time applications of the fabricated sensor. The development of biodegradable piezoelectric material and the fabrication of flexible sensors are as follows: first, a PLLA solution mixed with different weight percentages of Gly was prepared, and the solution was spin coated to get the piezoelectric thin films (Figure 1a). Subsequently, PLLA/Gly film was annealed at 80 °C for 30 min, followed by peeling it off from the glass slide. Then, to enhance the performance of piezoelectric biodegradable PLLA/Gly film, the content of glycine in PLLA was optimized (see Table S1, Supporting Information, methods), followed by choosing the optimal piezo film for further device demonstrations. Finally, the prepared piezoelectric PLLA/Gly film was sandwiched between two aluminum electrodes (top and bottom), and Kapton tape was used to encapsulate the sensor in order to minimize any errors in data measurement due to triboelectric effects (Figure 1b). The PLLA polymer and Gly combined as a result of hydrogen bonding between PLLA and Gly molecules, disintegrate in PBS solution as can be seen from reaction scheme (Figure 1c). The prepared piezoelectric PLLA/Gly film gradually degraded in PBS solution within 5 days at 37 °C (Figure 1d). The fabricated sensor was demonstrated as a wearable device for the detection of human pulse rate (carotid and radial artery) and other critical physiological signals such as wrist and elbow movement (bend and release), and swallowing and coughing actions (Figure 1e).

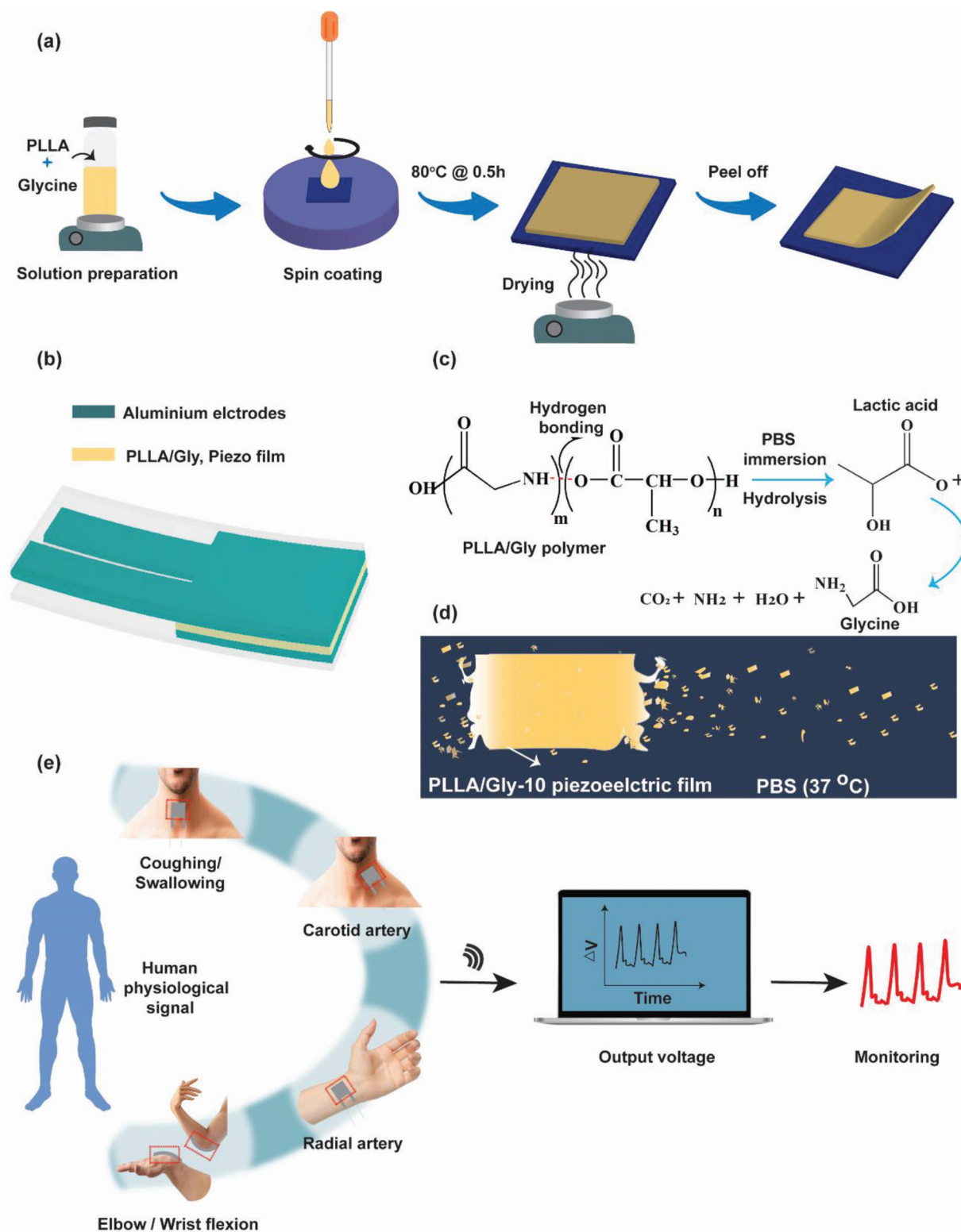


Figure 1. a) Schematic demonstration of the fabrication process for biodegradable piezoelectric PLLA/Gly film. A solution of PLLA/Gly spin-coated to get the desired thickness of the film ($\approx 15 \mu\text{m}$), followed by drying at 80°C for 30 min and peeling off from the glass slide. b) Schematic illustration of self-powered wearable sensor based on biodegradable piezoelectric film sandwiched between two aluminum electrodes and then encapsulated by polyimide tape (Kapton) to compactly sandwich the piezo film/Al assembly. c) Disintegration of PLLA/Gly polymer due to hydrolysis when immersed in PBS solution. d) Schematic illustration of PLLA/Gly piezoelectric film degradation in PBS solution at 37°C for 5 days. e) Schematic demonstration of the real-time applications of the flexible piezoelectric sensor in healthcare monitoring. Images of the body parts, along with a laptop, are created with freepik.com.

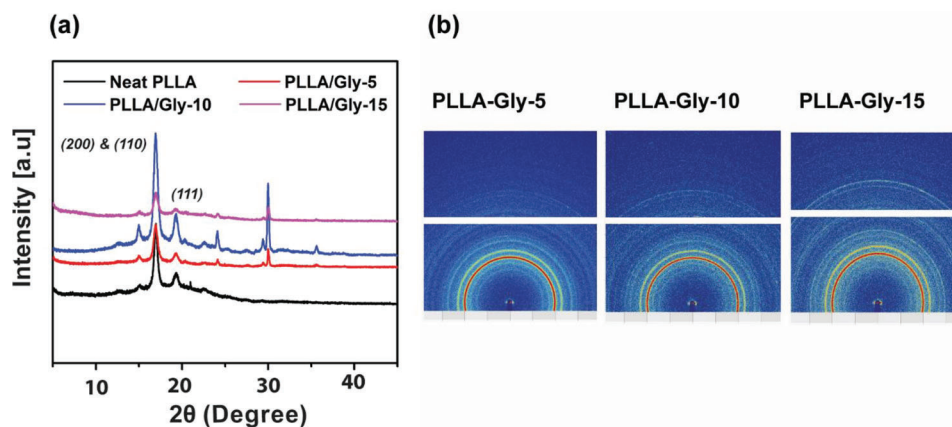


Figure 2. Characterization of crystallinity and polymer chain orientation for PLLA/Gly films. a) 1D XRD results for PLLA/Gly films with different weight% of glycine. b) 2D XRD photographs depict the orientation of the polymer chain of PLLA films with different glycine content.

In previous reports, amino acids have been used as heterogeneous nucleating agents to increase the crystallization rate and the degree of crystallinity of several polymers like PLA.^[55–61] In this way, the amount of Gly as a nucleating agent is optimized to increase the degree of crystallinity of PLLA. In addition, they do not affect the biodegradability of PLA. Glycine is a type of amino acid, and it has extensively been used in drug administration.^[62] Glycine comprises a backbone structure like PLLA with an acidic COOH group and a primary NH₂ group, but with different side chains. Maria et al. utilized glycine amino acid as a heterogeneous nucleating agent to analyze the impact of the isothermal crystallization behavior of PLA. They found that glycine possesses a substantial nucleating ability (54.1%).^[63] Incorporating glycine as a nucleating agent is preferred since PLLA and glycine are comprised of similar chemical structures enabling crystal formation.

The degree of crystallinity and orientation are two main properties of PLLA polymer that should be improved to induce piezoelectricity in PLLA.^[40,47] The piezoelectricity generated in PLLA under impact is due to the net polarization occurring due to the relative alignment of the C=O bond growing out from the PLLA backbone. To induce net polarization in PLLA, the molecular chains are required to be aligned in a similar direction forming an organized crystalline domain. In previous reports, researchers have used electrospun fibers of PLLA and a thermally drawn and compression-molded PLLA to develop flexible piezoelectric films.^[64–67] However, there were some major constraints, such as instability of the electrical signals generated from electro-spun membranes of PLLA under an applied force.^[64] Additionally, output signals are often mixed with the signals produced by the triboelectric effect (electric signals produced by the friction between electrodes and film).^[65]

Therefore, in this work, to obtain piezoelectric PLLA film without stretching or electrospinning PLLA, glycine (amino acid) is utilized to increase the degree of crystallinity of PLLA. X-ray diffraction (XRD) and differential scanning calorimetry (see Figure S2, Supporting Information) analysis was performed to study the crystallization behavior of PLLA and PLLA/Gly films. **Figure 2a** demonstrates the XRD patterns of neat PLLA and PLLA/Gly films. Neat PLLA (without glycine) shows three

broader peaks (amorphous nature) at 15°, 17°, and 19°, referring to the [010], [110]/[200], and [203] orientations of α -crystals, respectively.

Following the addition of glycine, PLLA exhibits three crystalline orientations [111], [200], and [110], and glycine crystal peaks are observed at 29.9° and 35.6°. With the addition of glycine content (i.e., 5, 10, and 15 wt% as of dry PLLA) in PLLA, the maximum intensity and sharpness of [200] and [110] peak were observed in the case of 10 wt% glycine content. This attributes to the transformation of α -form crystal structure having a left-handed 10₃ spiral shape to the β -form crystal formation having 3₁ spiral shape.^[68] In other words, the growing crystal structures are aligned or oriented more in [110] and [200] directions, turning it into piezoelectric PLLA (β -form). The increase in the intensity and sharpness of the glycine peak at 29.9° was also observed for the PLLA/Gly-10 sample. The XRD peak at 29.9° indicates the formation of the α -glycine phase, which is the thermodynamically more stable phase of the glycine.^[69] Glycine has three polymorphic phases (α , β , and γ) under ambient conditions. α -Glycine is known to have non-piezoelectric properties because of the centrosymmetric structure without piezoelectricity, while β -glycine and γ -glycine contain piezoelectric features owing to the non-centrosymmetric polar structure. Thus, the primary source of piezoelectricity is from treated PLLA (β -form). Utilizing XRD data, the degree of crystallinity of PLLA was also computed based on the ratio of area under the [200] and [110] peaks to the area under the whole curve (see Figure S3, Supporting Information). When the amount of glycine was increased to 15% by weight in PLLA, the intensity and sharpness of the peaks decreased, which might be due to the formation of glycine agglomerates. 2D-XRD analysis was conducted to estimate the orientation of crystalline structures after the addition of glycine. Likewise, a specific amount of glycine in PLLA enhances the degree of orientation of crystal domains, as shown in the 2D XRD image in Figure 2b. 2D-XRD photographs display the orientation of crystal domains inside PLLA, crystallized with glycine. The amorphous circle changes to a band as the film contains more aligned crystals. The less the sign band diverges from the axis, the more aligned the crystals film will have.^[67,70] As can be seen from the sample with 10 wt% glycine, less signal band diverges

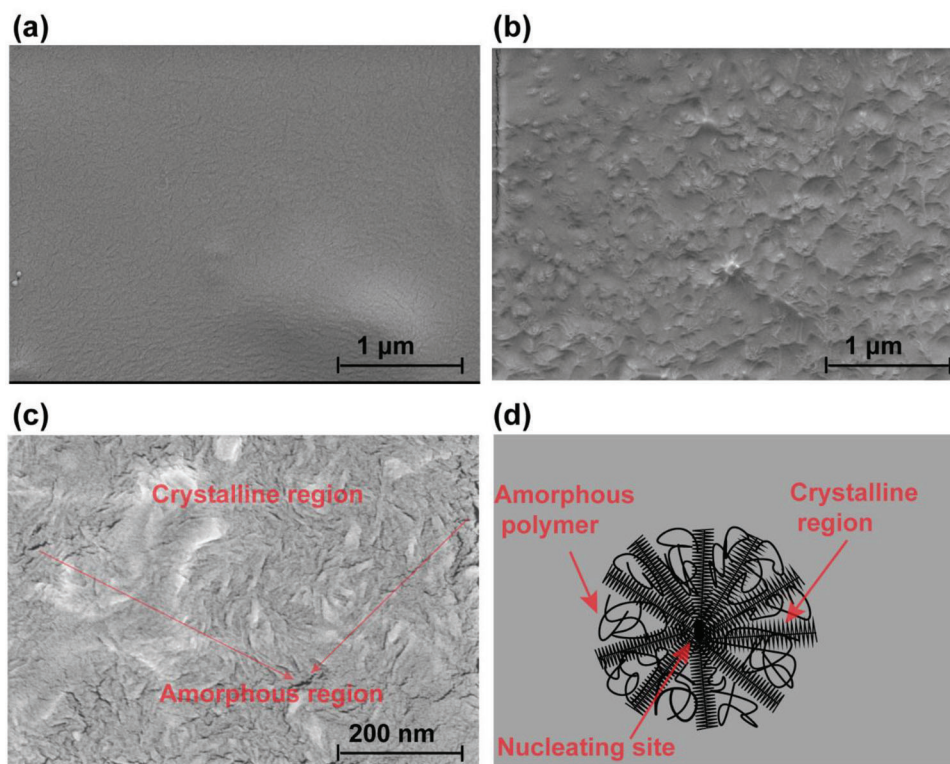


Figure 3. a–c) SEM images of crystallized PLLA/Gly-10 film at ambient conditions. d) Schematic illustration of crystalline structure comprises crystal lamellae connected by amorphous regions.

from the axis, which means it has a more aligned structure than other combinations. Herman's orientation function (f) commonly expresses the orientation degree, which symbolizes the average alignment of the pole relative to some reference orientation.^[71] With the addition of 10 wt% glycine in PLLA, the dispersion angle decreases while Herman's orientation function increases (see methods, Supporting Information). The data presented in Figure 2a agree with the 2D XRD results. These results describe an optimal weight percent of glycine (10 wt%) to obtain a flexible piezoelectric PLLA/Gly-10 film with improved crystallinity and a promising piezoelectric effect.

Furthermore, the crystallinity of α -crystals decreases, and the crystallinity of β -crystals increases, which could be due to the interaction between amine bonds in glycine and ester groups in PLLA. This subsequently improves the orientation of PLLA chains, ultimately increasing the crystallinity of β -form.^[72] Thus, the main source of piezoelectricity in PLLA/Gly composite film is from PLLA. We have analyzed FTIR spectroscopy of neat PLLA and composite samples to probe the interaction between PLLA and glycine (see Figure S4, Supporting Information). The interaction between PLLA and glycine and the formation of a hydrogen bond improves the chain alignment of the samples, possibly enhancing the piezoelectric properties of the PLLA/Gly composite.

PLLA is a semicrystalline polymer containing a significant part of an amorphous network but also comprises several crystal nuclei that rapidly grow with the addition of nucleating agents.^[73] The amorphous network of PLLA polymer is highly isotropic and retains a center of symmetry. In order to change the isotropic na-

ture of polymer chains to be piezoelectric, the center of symmetry must be eliminated.^[74] The addition of a very small amount of nucleating agent improves the crystallinity, accelerates the crystallization, and triggers a particular crystalline structure and morphology.^[75,76] Utilizing glycine content as nucleating agent results in introducing highly oriented new crystal structures. **Figure 3a–c** illustrates an SEM examination of the PLLA film surface with 10 wt% glycine content that displays the morphology of PLLA/Gly-10 composite film. The addition of 10 wt% glycine largely enhances the nucleation of PLLA by creating more nucleating sites, thus improving its crystallinity. The highly oriented crystal structures with the linear interface between them show that these structures nucleated simultaneously (Figure 3a,b). Numerous crystalline regions grown within the amorphous regions exhibit an organized orientation (Figure 3c). Likewise, an aligned network of polymer chains is anisotropic, an organized distribution of crystallites is also anisotropic. The intruding crystal structures having a nucleus in the center, and spread out dendritically from the nucleus, as depicted in Figure 3d.^[77] The orderly distribution of crystallite structure comprises crystal lamellae connected by amorphous regions of PLLA (Figure 3c,d).

Vibration and impact tests were conducted to assess the piezoelectric voltage outputs of the PLLA/Gly films under mechanical forces/strains, which have also been utilized for characterizing other piezoelectric materials.^[78,79]

The PLLA/Gly film was sandwiched between two aluminum electrodes and encapsulated in Kapton tape for vibration testing. The sensor was firmly affixed to the top portion of the aluminum beam with Kapton tape. Due to the triboelectric effects, Kapton

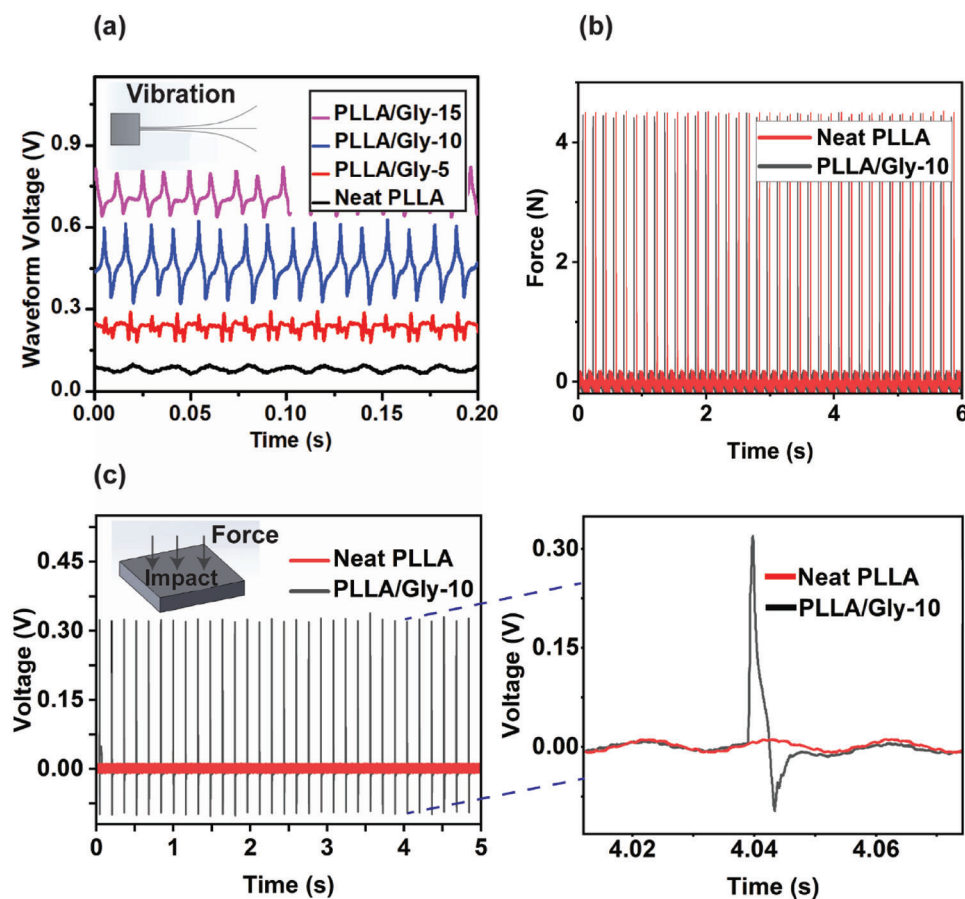


Figure 4. Measurement of piezoelectric PLLA/Gly output voltage from vibration and impact modes. a) Output voltage from neat PLLA and PLLA/Gly with different glycine content under vibration at 41 Hz. Simplified illustration of vibration setup used to get the output voltage (Inset). b) Same impact force applied to neat PLLA and PLLA/Gly-10. c) Output voltage from neat PLLA and PLLA/Gly-10 (left) subjected to the same force. Simplified schematic demonstration of impact setup (Inset of (c) [left]). (Right) enlarged view of output voltage.

tape was used to avoid errors in output signals. During the measurements, it was assured that the signals were not generated by triboelectricity or wire motion. The beam is fixed from one end, and the other side is attached to the electrodynamic shaker that controls the desired frequency and force levels (Supporting Information). The sensor is exposed to mechanical strains (Figure 4a, inset) by generating controlled oscillations using the setup. The impact testing system included a commercial force sensor (PCB) to measure the impact level, and the same electrodynamic shaker to produce dynamic forces on the PLLA/Gly-10 sensor (Figure 4c [left], inset). In both testing procedures, the sensor's output voltage is measured by a data acquisition system (NetdB DAQ12). Figure 4a shows open-circuit voltage outputs from PLLA films with different weight percent of glycine when it is subjected to vibration force at 41 Hz. Although the PLLA films with different percentage of glycine responded to the input with different piezoelectric response.

The neat PLLA film (control sample) produced only noise. The results show that the sample with 10 wt% of glycine in PLLA has the maximum signal output, showing the optimal amount of glycine. For the remaining measurements, the experiments were conducted only with piezo PLLA/Gly-10 film (10 wt% glycine as of dry PLLA) since significant piezoelectricity was acquired with

this sample. In addition, this film is uniform and highly flexible. Thus, for further characterization of the sensor, PLLA/Gly-10 was chosen as the optimal piezoelectric film. Figure 4b depicts that sensor fabricated from neat PLLA and PLLA/Gly-10 film was subjected to the same force level (≈ 4.5 N). Figure 4c (left) shows the open-circuit voltage output from the sensor fabricated with the optimal piezo film (PLLA/Gly-10) and neat PLLA. An input force of ≈ 4.5 N was applied to a sensor made by using optimal piezo film that resulted in a generation of peak-to-peak voltage output of ≈ 0.42 V, while the sensor made of neat PLLA resulted in only noise. The voltage output increased linearly with increasing applied force (see Figure S5, Supporting Information).

The piezoelectric output of the sensor increased almost linearly from ≈ 0.03 to ≈ 0.42 V under applied pressure ranging from 3.2 to 69.5 kPa (see Figure S5, Supporting Information).

The sensitivity, response time, and durability of the piezoelectric pressure sensor were characterized to validate the applicability of the sensor in detecting vital signals. Different known pressures/forces were applied, ranging from 3.2 to 69.5 kPa, on the piezoelectric sensor to calibrate output voltage. The distinct and clear output signals at different pressures permitted us to construct a calibration curve (Figure 5a). The calibration

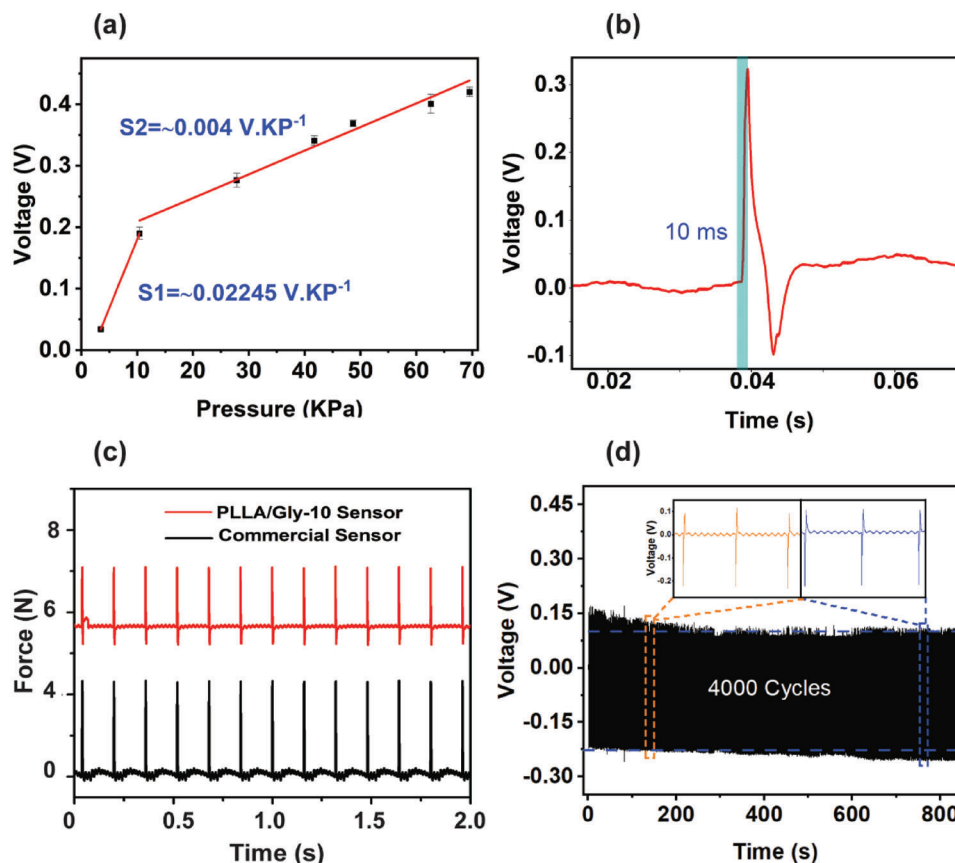


Figure 5. a) A typical calibration curve generated from PLLA/Gly-10 sensor under different input pressures. The piezoelectric sensor displays good linearity and sensitivity ranging from 3.2 to 69.5 kPa. b) Response time of PLLA/Gly-10. c) Output signals from commercial (PCB piezotronics sensor) and PLLA/Gly-10 sensor. d) Long-term (mechanical) durability test of the piezoelectric sensor under dynamic loading conditions with impact pressure of (31.25 kPa) and frequency of 5 Hz. The inset demonstrates an enlarged view of voltage output versus time.

curve could be useful for measuring pressures ranging from 0 to 69 kPa. Biodegradable piezoelectric PLLA/Gly-10 film could also be assembled with other metal electrodes such as silver, nickel, and gold for bio-compatible wearable applications. Moreover, biodegradable electrodes such as magnesium and molybdenum can also be used to fabricate a completely biodegradable piezoelectric sensor based on PLLA/Gly-10 film. Therefore, it could be utilized to measure physiological pressures such as intraocular pressure (0–5.3 kPa)^[80] and monitor diaphragmatic contraction.^[70]

The correlation between input pressure and voltage output can be described by two linear regions. Up to the 10 kPa pressure range, the slope obtained from the linear fit of voltage output is 0.02245 V kPa⁻¹, for example, the sensitivity of 0.02245 V kPa⁻¹. When the magnitude of pressure increases above 10 kPa, a slope of 0.004 V kPa⁻¹ is obtained from the linear fit of the voltage output, for example, a sensitivity of 0.004 V kPa⁻¹. The non-linear deformation of the PLLA/Gly-10 film as a function of input pressure may display two sensitivities. We computed the longitudinal piezoelectric charge coefficient d_{33} (expressed in pC N⁻¹) utilizing the following relation.^[81]

$$d_{33} = \frac{\epsilon_0 \epsilon_r}{d} \left(\frac{\Delta V}{\Delta P} \right) \quad (1)$$

where the thickness of the film, dielectric constant, and vacuum dielectric constant are represented as d , ϵ_r , and ϵ_0 (8.854×10^{-12} F m⁻¹) respectively. The sensitivity of the sensor is shown by $\Delta V/\Delta P$. The calculation of the dielectric constant is explained in method section of the Supporting Information. In this case, the value of ϵ_r was found to be 0.6192 at room temperature. Utilizing these values, the longitudinal piezoelectric charge coefficient, d_{33} , is estimated as ≈ 8 pC/N, which is in the range of previous reports.^[43] The response time refers to an increase in output voltage from the base point to the maximum point in response to the force applied to the sensor, which was assessed to be ≈ 10 ms upon pressure application. Whereas descent time is the recovery phase where output voltage reaches the base point when force is removed, which was calculated around ≈ 26 ms in our case. The recovery time (≈ 26 ms) (descent phase of peak) is slightly longer than the response time (ascent phase of peak), possibly because the device needs more time to recover from its shape change. Figure 5b depicts the response time of PLLA/Gly-10, for example, 10 ms, which is even faster than other pressure sensors (31–410 ms).^[82–84] This could be attributed to the high orientation of polymer chains and chemical stability of β -form of PLLA.

The accuracy of our sensor's signals is compared with a piezoelectric quartz force sensor (a commercially available PCB Piezotronics; 208C01). Utilizing the calibration curve plotted for

Table 1. Comparison of performance of different mechanical sensors.

Mechanism	Materials	Sensitivity	Self-powered	Response time [ms]	Durability	Ref.
Piezoresistance	Lead titanate (PbTiO ₃) nanowires/graphene	9.4×10^{-3} kPa ⁻¹	×	5–7	✓	[85]
	Graphene/paper	0.26 kPa ⁻¹	×	120	✓	[86]
	Polydimethylsiloxane (PDMS)/carbon nanotube	0.34 kPa ⁻¹	×	—	✓	[87]
Triboelectricity	Au nanowires/carbon nanotubes/PDMS	5.2 mV kPa ⁻¹	✓	—	✓	[88]
Piezoelectricity and triboelectricity	PEDOT:PSS/PTFE/PZT	5.7 mV kPa ⁻¹	✓	—	✓	[89]
Piezoelectricity	PVDF-ZnO	0.33 V kPa ⁻¹	✓	16	✓	[90]
	Nylone-11	0.13 mV kPa ⁻¹	✓	—	✓	[91]
	Polyacrylonitrile/PVDF	—	—	31	✓	[82]
	Collagen	27 mV N ⁻¹	✓	≈4.9	✓	[92]
	Chitosan/ β -glycine	2.82 ± 0.2 mV kPa ⁻¹	✓	—	✓	[69]
	Lithium niobate	28.8 nA kPa ⁻¹	✓	40	✓	[93]
	Imidazolium perchlorate (ImClO ₄)/ bacterial cellulose (BC)	4.24 mV kPa ⁻¹	✓	—	✓	[94]
	PLLA/Gly	13.2 mV kPa ⁻¹	✓	10	✓	This work

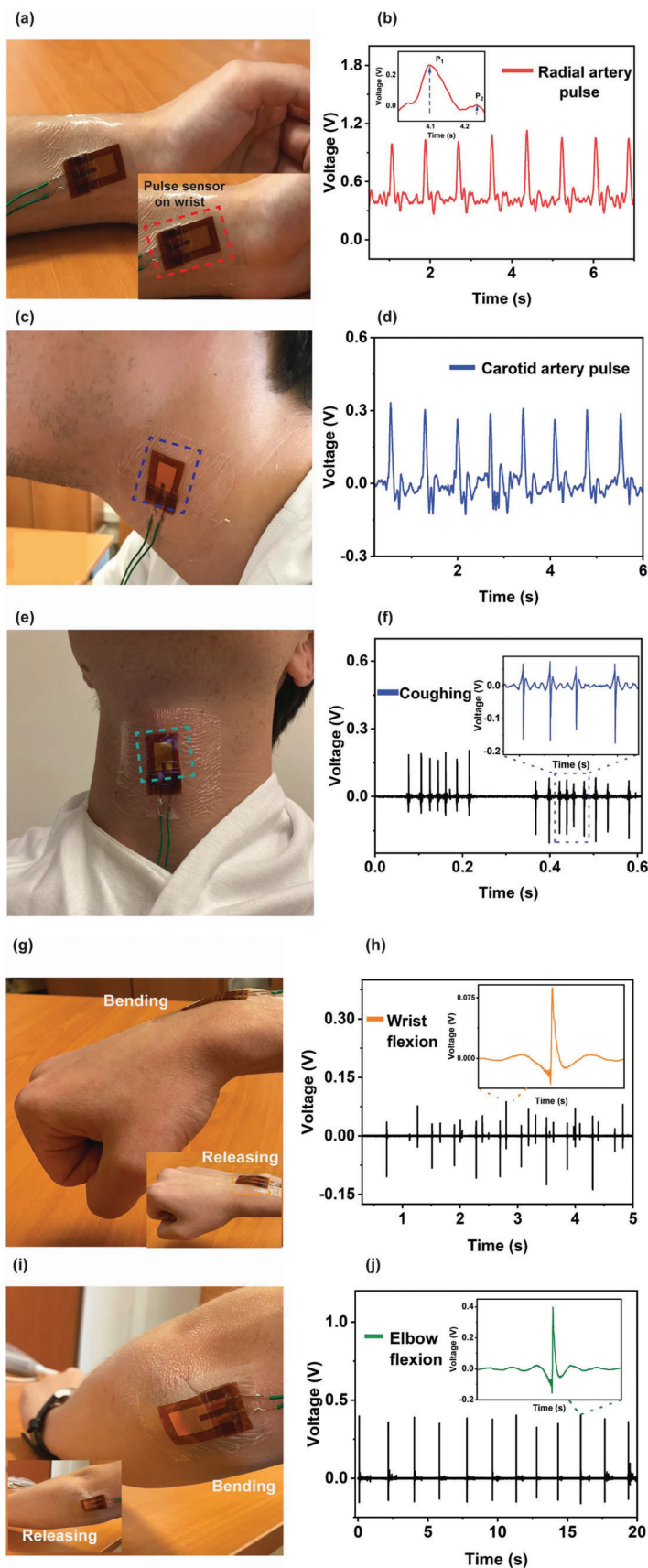
our sensor, the output voltage transformed to a force value. As shown in Figure 5c, the obtained signals closely correspond to the magnitude of applied force measured by the commercial sensor. Further, the sensor's long-term stability (mechanical durability) was assessed by applying dynamic pressure (31.25 kPa) over 4000 cycles at a 5 Hz frequency, as illustrated in Figure 5d. The voltage output response was relatively stable and displayed no major instability during periodic loading (see inset of Figure 5d). In this study, we focused on developing a biodegradable material-based piezoelectric sensor. We have compared the developed sensor with already existing sensors and presented them in Table 1. The developed bioresorbable piezoelectric film exhibits good sensitivity, response time, and considerable durability (Figure 5), which is better than most of the sensing devices mentioned in Table 1.

Moreover, the bioresorbable piezoelectric film possesses high sensitivity (13.2 mV kPa⁻¹) when compared to other bioresorbable piezoelectric materials.

Direct monitoring of physiological signals, including arterial pulse (radial and carotid) and muscle movement utilizing a piezoelectric sensor, has great potential in identifying human health information. Figure 6a displays a photograph of a piezoelectric sensor conformally affixed to the human wrist with a transparent adhesive thin film (3M Tegaderm) for detecting radial pulse rate. Stable deformation of the device results in effectively responding to the movement of blood vessels due to the good flexibility of the sensor (Movie S1, Supporting Information), as depicted in the inset of Figure 6a. A healthy male under 30 with no skin wounds, no allergic reactions, or ailments was considered for demonstrations. Approximately 72 beats per minute and an average voltage (V_{pp}) of 700 mV (with amplification, see ex-

perimental details (Supporting Information)) were generated by radial artery pulse. Important physiological and biomedical information, including blood pressure and arterial stiffness, can be inferred from the characteristic peaks of peripheral artery waveforms exhibited by an enlarged view of the pulse signal (inset of Figure 6b). In the normal state, peaks P_1 and P_2 indicate the sum of traveling and reflected waves (from the hand) and waves reflecting from the lower body deducted by the end-diastolic pressure, respectively. The difference in time of peaks P_1 and P_2 is denoted as ΔT_{DVP} , and the ratio of P_2 to P_1 is termed as radial artery augmentation index (AI_r), which strongly correlates with arterial stiffness.^[95] The average values measured for ΔT_{DVP} and AI_r were 0.15 and 1.05 s, respectively, which are compatible and correspond to a person under 30, as stated by Nichols.^[96] We then conformally attached the piezoelectric sensor to the human neck for non-invasive monitoring of other human physiological activities (Movie S2, Supporting Information), such as carotid artery pulse (Figure 6c). The voltage output (V_{pp}) generated from the carotid artery pulse (top panel, with amplification) was 400 mV, as demonstrated in Figure 6d. Using MATLAB, we applied low and bandpass filters to refine the data obtained for radial and carotid artery pulse using an oscilloscope (Rohde and Schwarz RTE 1034). More than 50 Hz of noise produced from the surrounding environments was refined using a low and band pass filter.

The device was then attached around the throat to detect the movement of muscles while coughing and drinking (Figure 6e; Movies S3 and S4, Supporting Information). The piezoelectric sensor shows high sensitivity to the movement of the esophagus muscle (the food pipe), allowing it to distinguish between signals produced by the esophagus during the vibration of the vocal



cord (coughing) (Figure 6f) and while drinking action (see Figure S6, Supporting Information). It could effectively detect the glottis' opening and closing physiological features during swallowing (Figure 6e).^[97] Thus, the wearable sensor could be useful in examining breath for the early detection of sudden infant death syndrome.^[98] Moreover, the sensor also showed high accuracy in detecting vocal cord vibration during the repetitive action of coughing. Thus, the wearable sensor can also be used to examine a patient's chronic obstructive pulmonary disease and damaged vocal cords, including chronic bronchitis and asthma, by evaluating the output signals of coughing action.^[97]

In addition, we attached the wearable piezoelectric sensor to the human wrist and elbow (Figure 6g–i; Movies S5 and S6, Supporting Information). Bending and releasing actions of both the wrist and the elbow led to the generation of clear voltage output signals due to the shear deformation of the piezoelectric film. Repetitive bending of the wrist and elbow produces a piezoelectric potential within the device, which generates a positive peak. A peak with negative amplitude appears upon release due to the reverse piezo potential (Figure 6h–j). This demonstration shows the tactile sensing capabilities of the wearable sensor during human activities. The wearable sensor could also power bioelectronics by harvesting small-scale mechanical energies. The power density and current output of the sensor are measured as a function of different resistances (R_L) ranging from 100 K Ω to 10 M Ω (under 6 Hz frequency) (see Figure S7, Supporting Information).

2.1. Biodegradation of PLLA/Gly-10 Film

In this study, we used non-degradable materials for encapsulation and electrodes to assess the piezoelectricity of biodegradable PLLA/Gly film due to the durability, flexibility, and easy fabrication method. Owing to the biodegradable nature of both the materials (PLLA and glycine) utilized in this study, it is important to estimate the rate of degradation of the PLLA/Gly film. The bioresorption of PLLA mainly depends on temperature and pH.^[99] Chen et al.^[100] reported that PLLA exhibits slow degradation in PBS (pH = 7.4) at room temperature, dropping only 5% of its initial weight after 6 weeks. They also demonstrated that the incorporation of other monomers into PLLA matrix significantly increased the degradation rate (lost more than 20% of initial weight). In this regard, degradation behavior of piezoelectric PLLA/Gly film was studied by submerging it in a PBS solution at 37 °C, as shown in Figure 7. Because of the slow bioresorption rate of PLLA in PBS with 7.4 pH, an accelerated degradation test was carried out at a pH of 12. The accelerated bioresorption test depicts the full dissolution of PLLA/Gly film in 5 days (Movie S7, Supporting Information). We investigated that the degradation rate of PLLA/Gly film in PBS (pH = 12), is higher than the degradation rate of PLLA in PBS (pH = 7.4).^[100] It can also be stated that the bioresorption rate of PLLA/Gly film enhanced sig-

nificantly due to the incorporation of glycine in PLLA matrix. This may be attributed to the hydrolysis of ester group as well as imine groups resulted in the degradation of PLLA/Gly which caused extra mass loss, while hydrolysis of the ester-bond backbone resulted in the degradation of PLLA.^[101]

3. Conclusion

In conclusion, we have successfully fabricated a wearable self-powered piezoelectric sensor based on a novel biodegradable piezoelectric material (PLLA/Gly-10) prepared by a simple and efficient method. The PLLA/Gly-10 thin film ($\approx 15 \mu\text{m}$) obtained by a spin coating process was sandwiched between two aluminum electrodes, followed by encapsulation with Kapton tape. The sensor demonstrated a sensitivity of ($\approx 0.01322 \text{ kPa}^{-1}$), 10 ms response time, and good long-term stability over 4000 impact cycles. The wearable sensor also responded to vibrations generated at 41 Hz. The sensor was conformally affixed to the human epidermis and monitored the radial/carotid artery pulse, human motion activities, and muscle movements. The acquired results suggest that PLLA/Gly-10 composite is a new promising biodegradable piezoelectric material for sensing applications. Compared with the sensor assembled with photolithography, the simple fabrication method makes the sensor more favorable. However, the fabrication method can be explored further to improve the piezoelectric properties. Furthermore, the biodegradable nature of the film makes the sensor a good alternative environment-friendly application, especially in healthcare applications where the maintenance of hygiene conditions is critical. Because of the biodegradability of piezoelectric PLLA/Gly film, it could be utilized to fabricate fully biodegradable/implantable biomedical devices for monitoring important bio-physiological pressures inside the body, allowing the development of new types of tissues and organs. In addition, the piezoelectricity of PLLA/Gly might be useful for generating voltage from biological deformations to offer an important electrical stimulation for the regeneration/repair of tissue, for example, wound healing.

4. Experimental Section

Dynamic Pushing Stage System: The vibration and impact tests were carried out by utilizing an electromechanical shaker (DP-V016, Data Physics Corporation) and function generator (3352A1, Agilent), which can modulate force and frequency rate.

Measurement of Electrical Characteristics: The output performance of the wearable piezoelectric sensor was conducted utilizing a data acquisition system (NetdB DAQ12) and a 4-channel oscilloscope (Rohde and Schwarz, RTE 1034). Two males under the age of 30 were considered for the real time monitoring of non-invasive physiological signals. The subjects read and signed the informed consent. Informed written consent from both the participants was obtained prior to the research.

Figure 6. a) Image of piezoelectric sensor conformally affixed to human wrist through a biocompatible adhesive (3M Tegaderm). The inset displays the wearable sensor consistent with the movement of the blood vessel. b) Signals detected by the PLLA/Gly-10 sensor from radial artery pulse, demonstrating different heart rates and produced voltage output under normal conditions. The inset shows enlarged voltage signals by the radial artery pulse, indicating pulse pressure (P_1) and late systolic augmentation (P_2). c) Image of piezoelectric sensor conformally affixed to the carotid artery position. d) The signals generated in response to the pressure produced by the carotid artery. e) Photograph of the piezoelectric sensor attached around the throat for monitoring strain instigated by muscle movement for the vibration of vocal cord (coughing (f)). Detected muscle movement in terms of voltage output. Photograph of the wearable piezoelectric sensor mounted on g) wrist and i) elbow joints. Detected joint motion in terms of voltage output h) wrist and j) elbow.

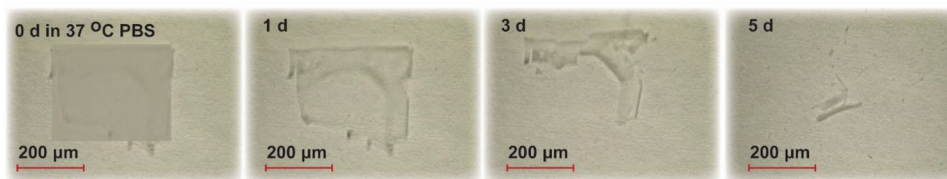


Figure 7. Optical images showing the biodegradability of piezoelectric PLLA/Gly film in PBS solution with time. The piezoelectric film completely degraded in PBS solution at 37 °C after 5 days.

Supporting Information

Supporting Information is available from the Wiley Online Library or from the author.

Acknowledgements

M.A., R.D., M.A., and L.B. was supported by The Scientific and Technological Research Council of Turkey (TUBITAK) through 2232 (#118C295) and European Research Council (#101043119). The authors acknowledge the use of the services and facilities of Koç University Surface Science and Technology Center (KUYTAM), Koç University Boron and Advanced Materials Application and Research Center (KUBAM), and n2STAR-Koç University Nanofabrication and Nano characterization Center for Scientific and Technological Advanced Research. The authors are thankful to Corbion biomaterials (The Netherlands) for providing the gift of Purasorb PL24. The authors are grateful to Dr. Yağız Morova, Dr. Mustafa Baris Yagci, and Dr. Hadi Jahangiri for their constructive comments and discussions. Also, the authors are very thankful to Dr. Emin Istif, Mohammad Javad Bathaei, Easa Aliabbasi, Engin Tarhan, Mujde Yahyaoglu, and Azmat Ullah for their help during the characterization.

Conflict of Interest

The authors declare no conflict of interest.

Data Availability Statement

The data that support the findings of this study are available from the corresponding author upon reasonable request.

Keywords

biodegradable devices, biodegradable piezoelectric polymers, carotid artery, health monitoring, radial artery

Received: April 2, 2023
Published online: May 19, 2023

- [1] C. Dagdeviren, Y. Shi, P. Joe, R. Ghaffari, G. Balooch, K. Usgaonkar, O. Gur, P. L. Tran, J. R. Crosby, M. Meyer, *Nat. Mater.* **2015**, *14*, 728.
- [2] L. Y. Chen, B. C.-K. Tee, A. L. Chortos, G. Schwartz, V. Tse, D. J. Lipomi, H.-S. P. Wong, M. V. McConnell, Z. Bao, *Nat. Commun.* **2014**, *5*, ncomms6028.
- [3] S. Imani, A. J. Bandodkar, A. M. Mohan, R. Kumar, S. Yu, J. Wang, P. P. Mercier, *Nat. Commun.* **2016**, *7*, 11650.
- [4] X. Wang, Y. Gu, Z. Xiong, Z. Cui, T. Zhang, *Adv. Mater.* **2014**, *26*, 1336.

- [5] J. T. Muth, D. M. Vogt, R. L. Truby, Y. Mengüç, D. B. Kolesky, R. J. Wood, J. A. Lewis, *Adv. Mater.* **2014**, *26*, 6307.
- [6] J.-W. Seo, M. Joo, J. Ahn, T.-I. Lee, T.-S. Kim, S. G. Im, J.-Y. Lee, *Nanoscale* **2017**, *9*, 3399.
- [7] Y. Wang, L. Wang, T. Yang, X. Li, X. Zang, M. Zhu, K. Wang, D. Wu, H. Zhu, *Adv. Funct. Mater.* **2014**, *24*, 4666.
- [8] M. Ma, Z. Zhang, Q. Liao, F. Yi, L. Han, G. Zhang, S. Liu, X. Liao, Y. Zhang, *Nano Energy* **2017**, *32*, 389.
- [9] H. He, H. Zeng, Y. Fu, W. Han, Y. Dai, L. Xing, Y. Zhang, X. Xue, *J. Mater. Chem. C* **2018**, *6*, 9624.
- [10] Y. Dai, Y. Fu, H. Zeng, L. Xing, Y. Zhang, Y. Zhan, X. Xue, *Adv. Funct. Mater.* **2018**, *28*, 1800275.
- [11] W. Gao, S. Emaminejad, H. Y. Y. Nyein, S. Challa, K. Chen, A. Peck, H. M. Fahad, H. Ota, H. Shiraki, D. Kiriya, *Nature* **2016**, *529*, 509.
- [12] S. Gong, W. Schwalb, Y. Wang, Y. Chen, Y. Tang, J. Si, B. Shirinzadeh, W. Cheng, *Nat. Commun.* **2014**, *5*, ncomms4132.
- [13] Y. Ma, Q. Zheng, Y. Liu, B. Shi, X. Xue, W. Ji, Z. Liu, Y. Jin, Y. Zou, Z. An, *Nano Lett.* **2016**, *16*, 6042.
- [14] Y. Mao, P. Zhao, G. McConohy, H. Yang, Y. Tong, X. Wang, *Adv. Energy Mater.* **2014**, *4*, 1301624.
- [15] C. Pan, L. Dong, G. Zhu, S. Niu, R. Yu, Q. Yang, Y. Liu, Z. L. Wang, *Nat. Photonics* **2013**, *7*, 752.
- [16] X. Wang, H. Zhang, L. Dong, X. Han, W. Du, J. Zhai, C. Pan, Z. L. Wang, *Adv. Mater.* **2016**, *28*, 2896.
- [17] X. Wang, M. Que, M. Chen, X. Han, X. Li, C. Pan, Z. L. Wang, *Adv. Mater.* **2017**, *29*, 1605817.
- [18] S. Jung, J. Lee, T. Hyeon, M. Lee, D. Kim, *Adv. Mater.* **2014**, *26*, 6329.
- [19] Q. Zheng, Y. Zou, Y. Zhang, Z. Liu, B. Shi, X. Wang, Y. Jin, H. Ouyang, Z. Li, Z. L. Wang, *Sci. Adv.* **2016**, *2*, e1501478.
- [20] M.-L. Seol, J.-W. Han, D.-I. Moon, M. Meyyappan, *Nano Energy* **2017**, *32*, 408.
- [21] Y. Zi, L. Lin, J. Wang, S. Wang, J. Chen, X. Fan, P. Yang, F. Yi, Z. L. Wang, *Adv. Mater.* **2015**, *27*, 2340.
- [22] S. H. Lee, C. K. Jeong, G.-T. Hwang, K. J. Lee, *Nano Energy* **2015**, *14*, 111.
- [23] F. Yi, Z. Zhang, Z. Kang, Q. Liao, Y. Zhang, *Adv. Funct. Mater.* **2019**, *29*, 1808849.
- [24] D. Lee, J. Chung, H. Yong, S. Lee, D. Shin, *Int. J. Precis. Eng. Manuf. - Green Technol.* **2019**, *6*, 43.
- [25] D. Y. Park, D. J. Joe, D. H. Kim, H. Park, J. H. Han, C. K. Jeong, H. Park, J. G. Park, B. Joung, K. J. Lee, *Adv. Mater.* **2017**, *29*, 1702308.
- [26] J. Mu, S. Xian, J. Yu, Z. Li, J. Zhao, J. Zhong, X. Han, X. Hou, J. He, X. Chou, *Sci. China: Technol. Sci.* **2022**, *65*, 858.
- [27] Y. Yang, H. Pan, G. Xie, Y. Jiang, C. Chen, Y. Su, Y. Wang, H. Tai, *Sens. Actuators, A* **2020**, *301*, 111789.
- [28] X. Chen, X. Li, J. Shao, N. An, H. Tian, C. Wang, T. Han, L. Wang, B. Lu, *Small* **2017**, *13*, 1604245.
- [29] S. Gong, B. Zhang, J. Zhang, Z. L. Wang, K. Ren, *Adv. Funct. Mater.* **2020**, *30*, 1908724.
- [30] C. Lee, T. Itoh, T. Suga, *IEEE Trans. Ultrason. Ferroelectr. Freq. Control* **1996**, *43*, 553.
- [31] C. W. Chee, C.-H. Wong, Z. Dahari, in *IEEE Region 10 Int. Conf., IEEE, Piscataway, NJ* **2016**, pp. 3771–3774.

- [32] H. Yuan, T. Lei, Y. Qin, R. Yang, *Nano Energy* **2019**, *59*, 84.
- [33] Y. Fu, H. He, T. Zhao, Y. Dai, W. Han, J. Ma, L. Xing, Y. Zhang, X. Xue, *Nano-Micro Lett.* **2018**, *10*, 76.
- [34] C. M. Boutry, A. Nguyen, Q. O. Lawal, A. Chortos, S. Rondeau-Gagné, Z. Bao, *Adv. Mater.* **2015**, *27*, 6954.
- [35] C. García Núñez, L. Manjakkal, R. Dahiya, *npj Flexible Electron.* **2019**, *3*, 1.
- [36] V. Nguyen, R. Zhu, K. Jenkins, R. Yang, *Nat. Commun.* **2016**, *7*, ncomms13566.
- [37] M. Minary-Jolandan, M.-F. Yu, *Biomacromolecules* **2009**, *10*, 2565.
- [38] A. Heredia, V. Meunier, I. K. Bdkin, J. Gracio, N. Balke, S. Jesse, A. Tselev, P. K. Agarwal, B. G. Sumpter, S. V. Kalinin, *Adv. Funct. Mater.* **2012**, *22*, 2996.
- [39] B. Y. Lee, J. Zhang, C. Zueger, W.-J. Chung, S. Y. Yoo, E. Wang, J. Meyer, R. Ramesh, S.-W. Lee, *Nat. Nanotechnol.* **2012**, *7*, 351.
- [40] M. Smith, Y. Calahorra, Q. Jing, S. Kar-Narayan, *APL Mater.* **2017**, *5*, 74105.
- [41] E. Fukada, *Jpn. J. Appl. Phys.* **1998**, *37*, 2775.
- [42] M. Ando, H. Kawamura, K. Kageyama, Y. Tajitsu, *Jpn. J. Appl. Phys.* **2012**, *51*, 09LD14.
- [43] Y. Tajitsu, S. Kawai, M. Kanesaki, M. Date, E. Fukada, *Ferroelectrics* **2004**, *304*, 195.
- [44] E. Fukada, *Biorheology* **1995**, *32*, 593.
- [45] J. Kobayashi, T. Asahi, M. Ichiki, A. Oikawa, H. Suzuki, T. Watanabe, E. Fukada, Y. Shikunami, *J. Appl. Phys.* **1995**, *77*, 2957.
- [46] Y. Ikada, Y. Shikunami, Y. Hara, M. Tagawa, E. Fukada, *J. Biomed. Mater. Res.* **1996**, *30*, 553.
- [47] M. Yoshida, T. Onogi, K. Onishi, T. Inagaki, Y. Tajitsu, *Jpn. J. Appl. Phys.* **2014**, *53*, 09PC02.
- [48] Y. Inuzuka, K. Onishi, S. Kinoshita, Y. Nakashima, T. Nagata, H. Yamane, T. Nakai, T. Kataoka, S. Ito, Y. Tajitsu, *Jpn. J. Appl. Phys.* **2012**, *51*, 09LD15.
- [49] J. Zhang, S. Gong, C. Wang, D. Jeong, Z. L. Wang, K. Ren, *Macromol. Mater. Eng.* **2019**, *304*, 1900259.
- [50] Y. Tajitsu, *Ferroelectrics* **2016**, *499*, 36.
- [51] M. Ando, H. Kawamura, H. Kitada, Y. Sekimoto, T. Inoue, Y. Tajitsu, *Jpn. J. Appl. Phys.* **2013**, *52*, 09KD17.
- [52] M. Ando, H. Kawamura, H. Kitada, Y. Sekimoto, T. Inoue, Y. Tajitsu, in *2013 Joint IEEE Int. Symp. on Applications of Ferroelectrics and Workshop on Piezoresponse Force Microscopy (ISAF/PFM 2013)*, IEEE, Piscataway, NJ **2013**, pp. 236–239.
- [53] C. M. Boutry, L. Beker, Y. Kaizawa, C. Vassos, H. Tran, A. C. Hincley, R. Pfattner, S. Niu, J. Li, J. Clavierie, *Nat. Biomed. Eng.* **2019**, *3*, 47.
- [54] J.-K. Chang, H.-P. Chang, Q. Guo, J. Koo, C.-I. Wu, J. A. Rogers, *Adv. Mater.* **2018**, *30*, 1704955.
- [55] K. S. Anderson, M. A. Hillmyer, *Polymer* **2006**, *47*, 2030.
- [56] S. C. Schmidt, M. A. Hillmyer, *J. Polym. Sci., Part B: Polym. Phys.* **2001**, *39*, 300.
- [57] H. Yamane, K. Sasai, *Polymer* **2003**, *44*, 2569.
- [58] H. Tsuji, H. Takai, N. Fukuda, H. Takikawa, *Macromol. Mater. Eng.* **2006**, *291*, 325.
- [59] H. Tsuji, H. Takai, S. K. Saha, *Polymer* **2006**, *47*, 3826.
- [60] N. Rahman, T. Kawai, G. Matsuba, K. Nishida, T. Kanaya, H. Watanabe, H. Okamoto, M. Kato, A. Usuki, M. Matsuda, *Macromolecules* **2009**, *42*, 4739.
- [61] J. Narita, M. Katagiri, H. Tsuji, *Macromol. Mater. Eng.* **2011**, *296*, 887.
- [62] N. Vale, A. Ferreira, J. Matos, P. Fresco, M. J. Gouveia, *Molecules* **2018**, *23*, 2318.
- [63] M. J. Carbone, M. Vanhalle, B. Goderis, P. Van Puyvelde, *J. Polym. Eng.* **2015**, *35*, 169.
- [64] G. Zhao, B. Huang, J. Zhang, A. Wang, K. Ren, Z. L. Wang, *Macromol. Mater. Eng.* **2017**, *302*, 1600476.
- [65] A. Sultana, S. K. Ghosh, V. Sencadas, T. Zheng, M. J. Higgins, T. R. Middy, D. Mandal, *J. Mater. Chem. B* **2017**, *5*, 7352.
- [66] S. J. Lee, A. P. Arun, K. J. Kim, *Mater. Lett.* **2015**, *148*, 58.
- [67] E. J. Curry, T. T. Le, R. Das, K. Ke, E. M. Santorella, D. Paul, M. T. Chorsi, K. T. M. Tran, J. Baroody, E. R. Borges, *Proc. Natl. Acad. Sci. U. S. A.* **2020**, *117*, 214.
- [68] J.-F. Ru, S.-G. Yang, D. Zhou, H.-M. Yin, J. Lei, Z.-M. Li, *Macromolecules* **2016**, *49*, 3826.
- [69] E. S. Hosseini, L. Manjakkal, D. Shakhthivel, R. Dahiya, *ACS Appl. Mater. Interfaces* **2020**, *12*, 9008.
- [70] E. J. Curry, K. Ke, M. T. Chorsi, K. S. Wrobel, A. N. Miller, A. Patel, I. Kim, J. Feng, L. Yue, Q. Wu, *Proc. Natl. Acad. Sci. U. S. A.* **2018**, *115*, 909.
- [71] M. Eguchi, M. S. Angelone, H. P. Yennawar, T. E. Mallouk, *J. Phys. Chem. C* **2008**, *112*, 11280.
- [72] S. K. Karan, S. Maiti, A. K. Agrawal, A. K. Das, A. Maitra, S. Paria, A. Bera, R. Bera, L. Halder, A. K. Mishra, *Nano Energy* **2019**, *59*, 169.
- [73] C. Ribeiro, V. Sencadas, C. M. Costa, J. L. G. Ribelles, S. Lanceros-Méndez, *Sci. Technol. Adv. Mater.* **2011**, *12*, 015001.
- [74] M. Smith, S. Kar-Narayan, *Int. Mater. Rev.* **2022**, *67*, 65.
- [75] G. Liu, X. Zhang, D. Wang, *Adv. Mater.* **2014**, *26*, 6905.
- [76] S. Saeidlou, M. A. Huneault, H. Li, C. B. Park, *Prog. Polym. Sci.* **2012**, *37*, 1657.
- [77] L. Gránásy, T. Pusztai, G. Tegze, J. A. Warren, J. F. Douglas, *Phys. Rev. E* **2005**, *72*, 11605.
- [78] D. A. Saravanos, P. R. Heyliger, D. A. Hopkins, *Int. J. Solids Struct.* **1997**, *34*, 359.
- [79] Q. Guo, G. Z. Cao, I. Y. Shen, *J. Vib. Acoust.* **2013**, *135*, 011003.
- [80] S. A. Bello, S. Malavade, C. L. Passaglia, *Ann. Biomed. Eng.* **2017**, *45*, 990.
- [81] D. B. Deutz, N. T. Mascarenhas, J. B. J. Schelen, D. M. de Leeuw, S. van der Zwaag, P. Groen, *Adv. Funct. Mater.* **2017**, *27*, 1700728.
- [82] R. Fu, L. Tu, Y. Zhou, L. Fan, F. Zhang, Z. Wang, J. Xing, D. Chen, C. Deng, G. Tan, *Chem. Mater.* **2019**, *31*, 9850.
- [83] C. R. Piedrahita, P. Yue, J. Cao, H. Lee, C. P. Rajapaksha, C. Feng, A. Jakli, T. Kyu, *ACS Appl. Mater. Interfaces* **2020**, *12*, 16978.
- [84] Y. Yue, N. Liu, W. Liu, M. Li, Y. Ma, C. Luo, S. Wang, J. Rao, X. Hu, J. Su, *Nano Energy* **2018**, *50*, 79.
- [85] Z. Chen, Z. Wang, X. Li, Y. Lin, N. Luo, M. Long, N. Zhao, J.-B. Xu, *ACS Nano* **2017**, *11*, 4507.
- [86] L.-Q. Tao, K.-N. Zhang, H. Tian, Y. Liu, D.-Y. Wang, Y.-Q. Chen, Y. Yang, T.-L. Ren, *ACS Nano* **2017**, *11*, 8790.
- [87] C. Ma, D. Xu, Y.-C. Huang, P. Wang, J. Huang, J. Zhou, W. Liu, S.-T. Li, Y. Huang, X. Duan, *ACS Nano* **2020**, *14*, 12866.
- [88] C. Ning, K. Dong, R. Cheng, J. Yi, C. Ye, X. Peng, F. Sheng, Y. Jiang, Z. L. Wang, *Adv. Funct. Mater.* **2021**, *31*, 2006679.
- [89] M. Zhu, Q. Shi, T. He, Z. Yi, Y. Ma, B. Yang, T. Chen, C. Lee, *ACS Nano* **2019**, *13*, 1940.
- [90] W. Deng, T. Yang, L. Jin, C. Yan, H. Huang, X. Chu, Z. Wang, D. Xiong, G. Tian, Y. Gao, *Nano Energy* **2019**, *55*, 516.
- [91] S. Anwar, M. Hassanpour Amiri, S. Jiang, M. M. Abolhasani, P. R. F. Rocha, K. Asadi, *Adv. Funct. Mater.* **2021**, *31*, 2004326.
- [92] S. K. Ghosh, D. Mandal, *ACS Sustainable Chem. Eng.* **2017**, *5*, 8836.
- [93] M. Xu, H. Kang, L. Guan, H. Li, M. Zhang, *ACS Appl. Mater. Interfaces* **2017**, *9*, 34687.
- [94] J. Lu, S. Hu, W. Li, X. Wang, X. Mo, X. Gong, H. Liu, W. Luo, W. Dong, C. Sima, Y. Wang, G. Yang, J. T. Luo, S. Jiang, Z. Shi, G. Zhang, *ACS Nano* **2022**, *16*, 3744.
- [95] S. Munir, B. Jiang, A. Guilcher, S. Brett, S. Redwood, M. Marber, P. Chowiecnyk, *Am. J. Physiol.* **2008**, *294*, H1645.
- [96] W. W. Nichols, *Am. J. Hypertens.* **2005**, *18*, 3.

- [97] P. Piirila, A. R. Sovijarvi, *Eur. Respir. J.* **1995**, *8*, 1949.
- [98] P. J. Fleming, R. Gilbert, Y. Azaz, P. J. Berry, P. T. Rudd, A. Stewart, E. Hall, *Br. Med. J.* **1990**, *301*, 85.
- [99] L. Xu, K. Crawford, C. B. Gorman, *Macromolecules* **2011**, *44*, 4777.
- [100] S. Chen, Y. Hao, W. Cui, J. Chang, Y. Zhou, *J. Mater. Sci.* **2013**, *48*, 6567.
- [101] Y. H. Kim, J. H. Park, M. Lee, Y.-H. Kim, T. G. Park, S. W. Kim, *J. Controlled Release* **2005**, *103*, 209.